FOURTH ORDER CRS STACK: SYNTHETIC EXAMPLES

P. Chira-Oliva, J. C. R. Cruz, M. Cardoso

email: *chira@ufpa.br*

keywords: *Fourth-order CRS, second-order CRS, ZO section*

ABSTRACT

The simulation of a zero-offset (ZO) seismic section from multi-coverage seismic data is a standard imaging method widely used in seismic processing that allows to reduces the amount of data and increases the signal-to-noise ratio. The CRS stacking method simulates ZO sections and does not dependent on a macro-velocity model. It is based on a second-order traveltime approximation parametrized with three kinematic wavefield attributes. In this work, we tested the Taylor expansion of the second-order CRS conventional operator, so-called the fourth-order CRS stacking operator, to simulate ZO seismic sections. This formula depends on the same three parameters as the second-order CRS operator. Synthetic examples have shown a good performance of the proposed expression compared to the CRS conventional operator.

INTRODUCTION

The seismic stacking is performed along traveltime moveout expressions (curves or surfaces) that depend on one or more parameters. As result of the stacking process, one obtains, besides a stacked section of improved image quality and attribute sections that can be used for further processing.

In the last years, have appeared diverse methods as a new alternative or to generalize the Common-midpoint (CMP) stacking method. These methods are referred in the literature as macro-model independent or data driven methods (Hubral, 1999). Instead of working only with one kinematic parameter or the stacking velocity (CMP method), the new methods provide two or three parameters for each point of the simulated ZO section.

The Common-Reflection-Surface (CRS) method belongs to this group. This method sums the amplitudes of the seismic traces in the multi-coverage data along the surface defined by the hyperbolic traveltime approximation in the form derived in Tygel et al. (1997). Thus, we call this formula as the second-order CRS or conventional CRS operator. This operator depends on three parameters: the emergence angle of the normal ray (with respect to the measurement surface normal) and the wavefront curvatures of the two hypothetical waves, called Normal-Incidence-Point (NIP) wave and Normal (N) wave introduced by Hubral (1983). For the CMP configuration, these parameters reduce for the Normal-moveout (NMO) velocity parameter.

The CRS stacking method follows a more general approach that considers the location, orientation and curvatures of reflector segments setting up the interfaces.

In the search of a more accurate traveltime approximation or operator, Höcht et al. (1999) derived a Taylor expansion of the second-order CRS operator, so-called the fourth-order CRS operator. This new CRS operator is described in terms of the same parameters of the conventional CRS operator.

Chira-Oliva et al. (2003) reviewed the derivation of the fourth-order CRS operator and discussed first comparisons for different seismic configurations with the second-order CRS operator by considering synthetic models. They suggested that this high-order operator can provide a better approximation to true traveltimes of reflection or diffraction events than the conventional CRS operator.

Cardoso (2008) tested the fourth-order CRS operator on simple synthetic models to simulate zero-offset sections. He obtained good results from the investigated CRS operator when compared with the conventional CRS operator.

In this work, we tested the Taylor expansion of the conventional CRS operator, so-called the fourth-order CRS stacking operator, to simulate ZO seismic sections. Synthetic examples have shown a good performance of the proposed expression compared to the CRS conventional operator by considering larger offsets.

THEORY

Reflection events

We assume that multi-coverage data are acquired on a single horizontal seismic line. On this line, we consider a fixed ZO primary reflection ray or central ray. This ray is specified by the coordinate x_0 that locates the coincident source-receiver pair. Paraxial primary reflection rays in the vicinity of the central ray are specified by their midpoint and half-offset coordinates (x_m, h). The traveltime of the two-way ZO central ray is denoted by t_0. The wavefront curvatures, K_N and K_{NIP}, refer to the normal (N) wave and normal-incident-point (NIP) wave, respectively. We assume that the CRS parameters (β_0, K_{NIP}, K_N) are known. For a paraxial ray specified by the coordinates (x_m, h), the second-order CRS operator (Tygel et al., 1997) is given by

$$t_2^2(x_m,h) = \left(t_0 + 2\,\frac{\sin\beta_0}{v_0}\,(x_m - x_0)\right)^2 + \frac{2\,t_0\,\cos^2\beta_0}{v_0}\left(K_N\,(x_m-x_0)^2 + K_{NIP}\,h^2\right)\,. \quad (1)$$

The fourth-order CRS operator (Höcht et al., 1999) is based on the construction of the exact traveltime formula for the case of an inhomogeneous medium where they assumed an emerging wave circular, defined by the emergence angle β_0 and the radius of curvature of the true wave observed at x_0. This wave propagates with a constant velocity v_0 near to the surface. This operator has the form

$$\begin{aligned} t_4^2(x_m,h) =& t_2^2(x_m,h) \\ &+ \frac{\cos^2\beta_0}{v_0^2}\left[A\,(x_m-x_0)\,h^2 + B\,(x_m-x_0)^3 + C\,(x_m-x_0)^4 + D\,(x_m-x_0)^2\,h^2 + E\,h^4\right]. \end{aligned} \quad (2)$$

being

$$\begin{aligned} A &= 2K_{NIP}\sin\beta_0(2 - 2v_0t_0K_N - 2v_0t_0K_{NIP})\,, \\ B &= 2K_N\sin\beta_0(2 - v_0t_0K_N)\,, \\ C &= K_N^2\left(5\cos^2\beta_0 - 4)(1 - \frac{v_0t_0K_N}{2}\right)\,, \\ D &= K_{NIP}(2v_0t_0[3 - 4\cos^2\beta_0]K_N^2 + K_N[4 - 5\cos^2\beta_0][-2 + v_0t_0K_{NIP}] \\ &\quad - 2K_{NIP}\sin^2\beta_0[2 - v_0t_0K_{NIP}])\,, \\ E &= K_{NIP}^2[2v_0t_0K_N\sin^2\beta_0 - (v_0t_0K_{NIP}\cos^2\beta_0)/2 + \cos^2\beta_0]\,. \end{aligned} \quad (3)$$

Up to the second order both equations reduce to formulae obtained by paraxial ray theory (Schleicher et al., 1993). These CRS operators are shown for a 2-D model (Figure 1).

Seismic configurations

For important seismic configurations, the above formulas reduce to simpler forms.

Common-midpoint (CMP) configuration

For this configuration, we have $x_m = x_0$. Consequently, the fourth-order CMP traveltime is given by

$$t^2_{4,CMP}(h) = t_0^2 + \frac{2\ t_0\ \cos^2\beta_0}{v_0}\ K_{NIP}\ h^2 + \frac{\cos^2\beta_0}{v_0^2}\ E\ h^4\ . \tag{4}$$

Zero-Offset (ZO) configuration

The ZO configuration is characterized by the condition $h = 0$. The fourth-order ZO traveltime is given by

$$\begin{aligned} t^2_{4,ZO}(x_m) =& [t_0 + \frac{2\ \sin\beta_0}{v_0}\ (x_m - x_0)]^2 \\ &+ \frac{2\ t_0 \cos^2\beta_0}{v_0}\ K_N\ (x_m - x_0)^2 + \frac{\cos^2\beta_0}{v_0^2}(B\ (x_m - x_0)^3 + C\ (x_m - x_0)^4)\ . \end{aligned} \tag{5}$$

Diffraction events

For a pure diffraction, i.e., the situation in which the reflector reduces to a single diffraction point. In this case the NIP and N waves are coincident, i.e. both propagate from a point source at NIP and have identical radii of curvatures at X_0, $K_{NIP} = K_N$. As a consequence, equations (1) and (2) becomes

$$t^2_{2,diff}(x_m, h) = \left(t_0 + 2\ \frac{\sin\beta_0}{v_0}\ (x_m - x_0)\right)^2 + \frac{2\ t_0\ \cos^2\beta_0}{v_0}\left(K_{NIP}\ [(x_m - x_0)^2 + h^2]\right)\ , \tag{6}$$

and

$$\begin{aligned} t^2_{4,diff}(x_m, h) =& t^2_{2,diff}(x_m, h) \\ &+ \frac{\cos^2\beta_0}{v_0^2}\ [A_1\ (x_m - x_0)\ h^2 + B_1\ (x_m - x_0)^3 + C_1\ (x_m - x_0)^4 \\ &+ D_1\ (x_m - x_0)^2\ h^2 + E_1\ h^4]\ . \end{aligned} \tag{7}$$

being

$$\begin{aligned} A_1 &= 2K_{NIP}\sin\beta_0(2 - 4v_0t_0K_{NIP})\ , \\ B_1 &= 2K_{NIP}\sin\beta_0(2 - v_0t_0K_{NIP})\ , \\ C_1 &= K^2_{NIP}\left(5\cos^2\beta_0 - 4)(1 - \frac{v_0t_0K_{NIP}}{2}\right)\ , \\ D_1 &= K_{NIP}(2v_0t_0[3 - 4\cos^2\beta_0]K^2_{NIP} + K_{NIP}[4 - 5\cos^2\beta_0][-2 + v_0t_0K_{NIP}] \\ &- 2K_{NIP}\sin^2\beta_0[2 - v_0t_0K_{NIP}])\ , \\ E_1 &= K^2_{NIP}[2v_0t_0K_{NIP}\sin^2\beta_0 - (v_0t_0K_{NIP}\cos^2\beta_0)/2 + \cos^2\beta_0]\ . \end{aligned} \tag{8}$$

being both equations the second-order and fourth-order Common-Diffraction-Surface (CDS) operators, respectively.

SYNTHETIC EXPERIMENTS

To test both CRS operators with respect its potential for ZO simulation of seismic sections, we created a synthetic model.

2-D model

The model is constituted of two homogeneous layers above a half-space. The acquisition is lying on a horizontal line (Figure 2). Based on this model, we generated a synthetic data set of multi-coverage primary reflections, using the ray-tracing algorithm, SEIS88 (Cerveny and Psensik, 1988). The data do not

have noise and were created according a common-shot (CS) configuration. The maximum offset was 4 km. The source signal was a Gabor wavelet with 40 Hz dominant frequency and the time sampling was 25ms. Figure 3a shows the ray-theoretical modelled ZO section without noise. Figure 3b shows the simulated ZO section that results from the application of the second-order CRS stacking operator. Figure 3c shows the simulated ZO section that results from the application of the fourth-order CRS stacking operator. We also compared the seismic trace at the location x_0 = 1.05 km for the ZO sections obtained by the ray-theory and the CRS operators, second and fourth-order (Figures 4). We have compared the capability of the second and fourth-order CRS traveltime expansions to simulate ZO seismic sections. As we can clearly see, the fourth-order approximation presents enhanced primary reflection events, with larger S/N that the corresponding one in the modelled ZO section. For the other results, the fourth-order formula generally provides better approximation than the second-order CRS expression.

CONCLUSIONS

We propose the fourth-order CRS traveltime expansion as a new alternative for the seismic stacking. The fourth-order CRS operator tested on simple synthetic models provide good stacked sections with a higher S/N. Then, the investigated CRS operator is useful to provide simulated ZO sections. This traveltime expression depends on the same three parameters as its conventional CRS traveltime expression or second-order CRS operator. Our first results provides good stacked sections within a significantly larger aperture than the conventional CRS operator.

ACKNOWLEDGMENTS

The third author thanks the Brazilian National Research Council (CNPq) for the scholarship. We also thank the sponsors of the Wave Inversion Technology (WIT) Consortium (Germany) for their support.

REFERENCES

Cardoso, M. (2008). Imaging of seismic reflectors by using the fourth-order Common-Reflection-Surface CRS operator (in portuguese). *Graduation in Geophysics, Federal University of Pará (UFPA - Brazil)*, pages 1–52.

Cerveny, V. and Psensik, I. (1988). *Ray Tracing program*. Charles University, Czechoslovakia.

Chira-Oliva, P., Tygel, M., Hubral, P., and Schleicher (2003). A fourth-order CRS moveout for reflection or diffraction events: numerical examples. *Journal of Seismic Exploration*, 12:197–219.

Höcht, G., de Bazelaire, E., P., M., and Hubral, P. (1999). Seismic and optics: hyperbolae and curvatures. *Journal of Applied Geophysics*, 42:261–281.

Hubral, P. (1983). Computing true amplitude reflections in a laterally inhomogeneous earth. *Geophysics*, 48:1051–1062.

Hubral, P. E. (1999). Macro-model independent seismic reflection imaging. *Journal of Applied Geophysics, Special Issue*, 42:137–346.

Schleicher, J., Tygel, M., and Hubral, P. (1993). Parabolic and hyperbolic paraxial two-point traveltimes in 3D media. *Geophysical Prospecting*, 41(4):459–513.

Tygel, M., Muller, T., Hubral, P., and Schleicher, J. (1997). Eigenwave based multiparameter traveltime expansions. *Expanded Abstracts, 67th Ann. Internat. SEG Mtg., Dallas*, pages 1770–1773.

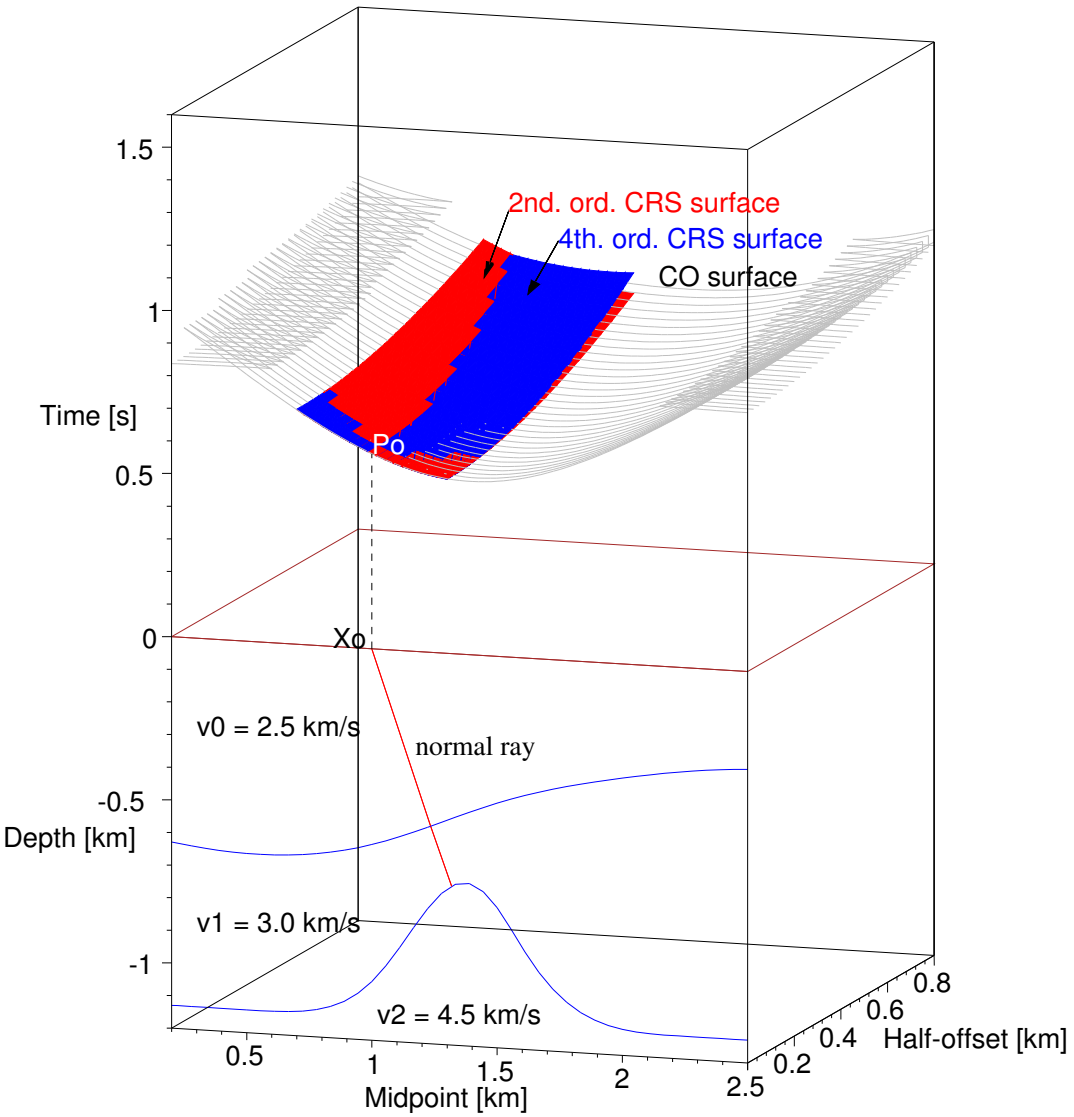

Figure 1: Bottom: model consisting of two homogeneous layers above a half-space. Top: Forward-calculated multi-coverage traveltime surface (gray) compared with the 2nd-order (red) and 4th-order (blue) CRS stacking operators for a reflection point according to the true attributes.

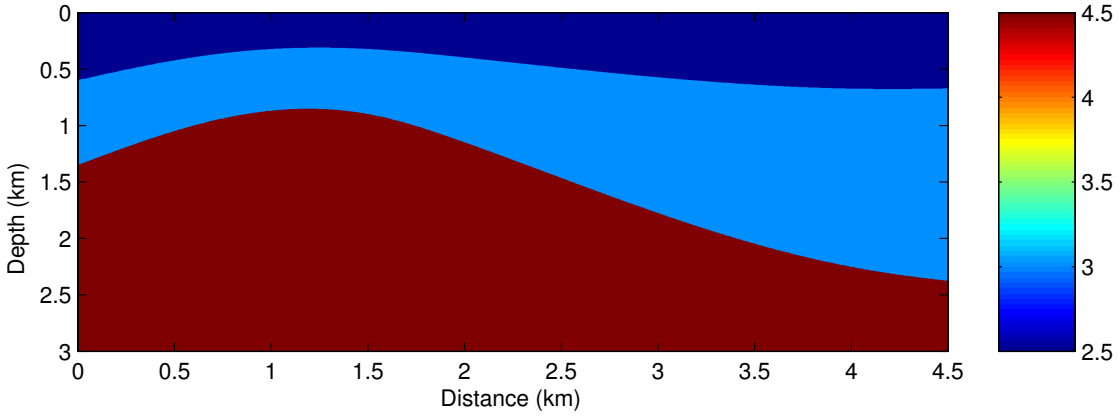

Figure 2: 2-D model constituted of two isovelocity layers about a half-space with curved interface. Interval velocities are 2.5 km/s, 3.0 km/s and 3.5 km/s, respectively.

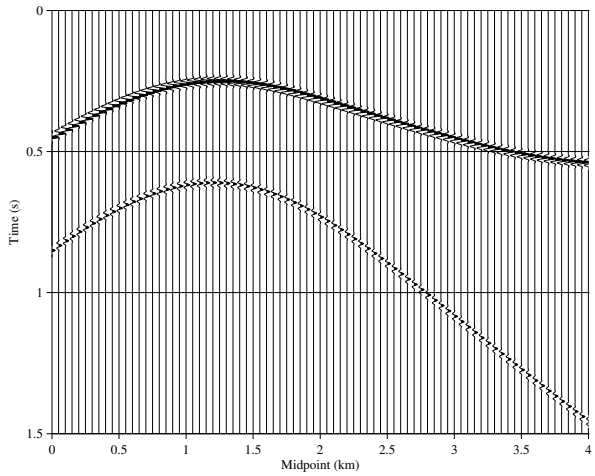

(a)

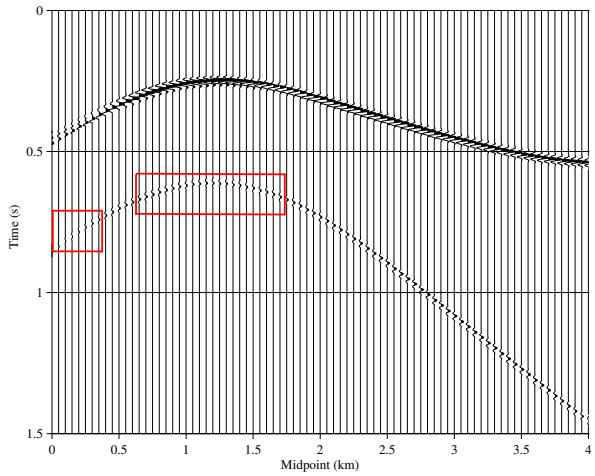

(b)

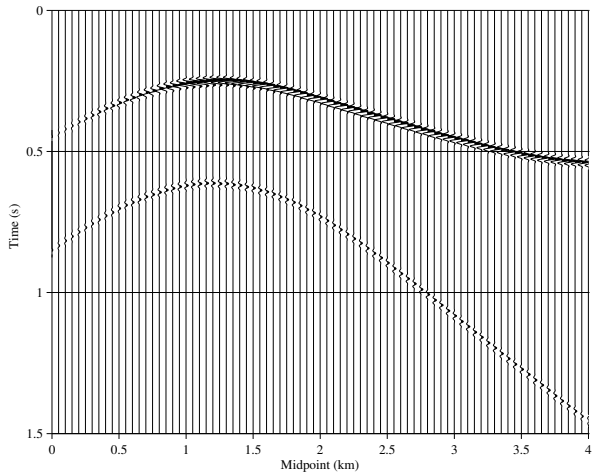

(c)

Figure 3: a)ZO section obtained by forward modelling (Figure 2). b)Simulated ZO section with the second-order CRS stack by using the multi-coverage seismic data. c)Simulated ZO section with the fourth-order CRS stack by using the multi-coverage seismic data. In red boxes, the fourth-order CRS operator simulates better the ZO traces than the second-order CRS operator.

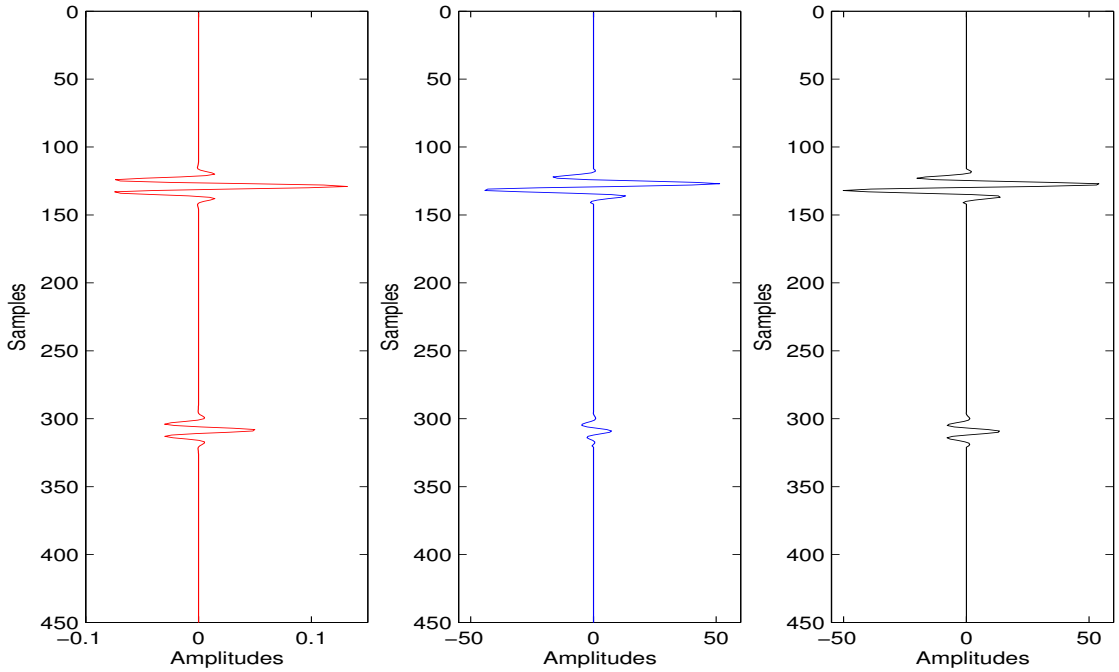

(a)

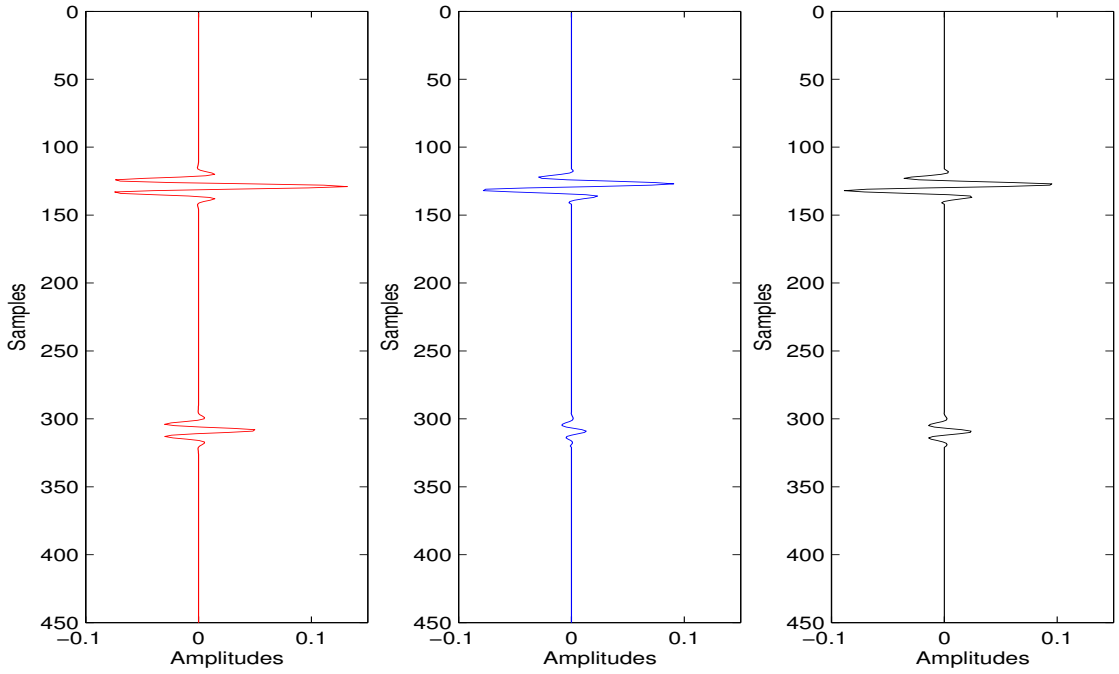

(b)

Figure 4: a)Comparison of the simulated ZO seismic traces at x_0=1.05 km (Figure 3): Forward modelling (left), 2nd-order CRS (middle) and 4th-order CRS (right). b)Comparison of the simulated ZO seismic traces and normalized by the number of traces at x_0=1.05 km: Forward modelling (left), second-order CRS (middle) and fourth-order CRS (right).